The Role of Climate and Vegetation in Regulating Drought–Heat Extremes

Sungmin O,[a,b] Ana Bastos,[a] Markus Reichstein,[a] Wantong Li,[a] Jasper Denissen,[a] Hanna Graefen,[a] and Rene Orth[a]

[a] Max Planck Institute for Biogeochemistry, Jena, Germany
[b] Department of Climate and Energy System Engineering, Ewha Womans University, Seoul, South Korea

ABSTRACT: Droughts cause serious environmental and societal impacts, often aggravated by simultaneously occurring heat waves. Climate and vegetation play key roles in the evolution of drought-associated temperature anomalies, but their relative importance is largely unknown. Here, we present the hottest temperature anomalies during drought in subhumid and tree-dominated regions using observation-based, global data over 2001–15. These anomalies are mainly driven by a drought-related net radiation surplus and further amplified by forests' water-saving strategies that result in diminished evaporative cooling. By contrast, in semiarid and short-vegetation regions, drought-related temperature increases are smaller. The reduction of evaporative cooling is weak and net radiation increases only marginally due to high albedo over drought-stressed vegetation. Our findings highlight the importance of considering all interacting factors in understanding diverse mechanisms of concurrent drought–heat extremes across different climate regimes.

SIGNIFICANCE STATEMENT: Climate and vegetation have a strong influence in regulating temperature anomalies during drought. However, the physical mechanisms behind drought–heat events across different climate–vegetation regimes are not always accurately described in physically based models. Here we use global-scale, observation-based datasets to show the spatial variation of temperature anomalies during drought, with the largest anomalies in subhumid and tree-dominated regions. Further, we present observational evidence for the relative roles of climate and vegetation in shaping drought–heat extremes across space. Our study provides valuable inputs to better understand the drought–heat pathways and their spatial variations, which can inform drought adaptation and mitigation efforts.

KEYWORDS: Drought; Extreme events; Atmosphere-land interaction; Hydrometeorology

1. Introduction

Drought is considered to be the most complex and least understood of all climate extremes, affecting large areas and populations (Wilhite 2000; Below et al. 2007). Prolonged drought can disrupt agricultural activities and ecosystems (Bastos et al. 2020), threaten water and energy security (Shadman et al. 2016), and increase fire hazards (O et al. 2020b). Drought often induces elevated temperatures. Such concurrent drought and heat events can exacerbate environmental and societal impacts anticipated from individual drought events, as witnessed during 2003 in Europe (Fink et al. 2004; Ciais et al. 2005) and 2010 in Russia (Hauser et al. 2016; Flach et al. 2018). Substantial increases in the frequency of concurrent drought and heat extremes have recently been reported in many regions of the world (Mazdiyasni and AghaKouchak 2015; Sharma and Mujumdar 2017; Alizadeh et al. 2020; Yu and Zhai 2020). Furthermore, climate model projections suggest amplified warming of droughts in the future (Chiang et al. 2018; Cheng et al.

2019). Thus, understanding the underlying mechanisms responsible for drought-induced heat is crucial to inform drought management strategies and to improve the prediction of dry–hot extremes, especially under a changing climate.

The role of soil moisture in linking drought and heat has been well recognized. Prior studies, although constrained by the use of proxy indices or limited amounts of in situ data, have provided ample evidence that low soil moisture during drought events suppresses evaporative cooling, subsequently resulting in increased local temperatures (Hirschi et al. 2011; Mueller and Seneviratne 2012; Teuling 2018). However, drought-induced heat (drought–heat) cannot be solely attributed to soil moisture deficits. Changes in local land cover during droughts, such as dried soils or dead grasses, and diverse responses of different vegetation types to drought can also affect the drought–heat relationship (Lobell and Asner 2002; Teuling and Seneviratne 2008; Matheny et al. 2015; Anderegg et al. 2019; Grossiord et al. 2020; Tollerud et al. 2020). However, a comprehensive assessment of the relevant land surface components and their contributions to drought–heat extremes is still lacking.

Moreover, the relationship between the large-scale spatial variation of drought-induced heat and background bioclimatic conditions is so far unresolved, owing largely to a lack of suitable

🔓 Denotes content that is immediately available upon publication as open access.

🔗 Supplemental information related to this paper is available at the Journals Online website: https://doi.org/10.1175/JCLI-D-21-0675.s1.

Corresponding author: Sungmin O, sungmino@bgc-jena.mpg.de

land surface data. Likewise, the drought–heat processes described in process-based models remain uncertain due to the imperfect representation of relevant land surface interactions (Santanello et al. 2018; Miralles et al. 2019). Here, we overcome this limitation by employing global soil moisture and latent heat (=evaporative cooling) data generated from respective in situ measurements through a data-driven approach.

We examine daily maximum temperature anomalies during extreme droughts and show a systematic spatial variability of corresponding net radiation and latent heat anomalies across climatic regimes. We further demonstrate the contrasting role of trees and short vegetation on drought–heat pathways, especially in transitional regimes (subhumid and semiarid climates). Consequently, our comprehensive assessment using multiple variables disentangles the relative roles of climate and vegetation in shaping drought–heat extremes across space.

2. Data and methods

a. Data

Soil moisture data are obtained from the SoMo.ml, a global soil moisture dataset generated using a machine learning (ML)-based model (O and Orth 2021). The ML-based model was trained to simulate daily temporal dynamics learned from the in situ measurements. Data are available for three different soil layers on a 0.25° × 0.25° latitude–longitude grid. We upscaled the data with linear interpolation into 0.5° × 0.5° and then vertically interpolated to the depth of 0–50 cm. SoMo.ml v1.0 is publicly available via https://doi.org/10.17871/bgi_somo.ml_v1_2020.

Latent heat data are from FLUXCOM, which is generated through multiple ML algorithms trained with energy flux measurements from FLUXNET eddy covariance towers (Jung et al. 2019). We selected latent heat ensemble from the remote sensing setup, where fluxes are estimated exclusively from MODIS satellite data. More information about the data can be found from http://www.fluxcom.org/. Data are available at a 0.5° spatial resolution for the period of 2001–15. Eight-daily data are linearly interpolated to a daily scale, which can possibly underestimate daily extreme values; however, this would not significantly affect our results.

We additionally employ latest version of the ECMWF global reanalysis data (ERA5; Hersbach et al. 2020) to obtain daily net radiation and daily maximum temperature. Those are relatively well constrained with observations such as synoptic station data and satellite radiances through the data assimilation. The data are available at a daily scale and interpolated to a 0.5° grid.

Diverse data sources are considered in our study so that the employed datasets can be largely independent of each other. Moreover, both the reanalysis and ML-driven data used in this study substantially rely on observations. While the reanalysis combines physically based model data with observations, the ML-driven datasets are based on process knowledge established purely from the observational training data.

b. Drought event selection

Drought peaks are defined as consecutive days with the lowest mean soil moisture (5-day moving window). The day

corresponding to the drought peak over the period of 2001–15 is selected per each grid pixel (0.5° × 0.5°). We discard grid pixels where the long-term-mean temperature is lower than 5°C or where the aridity index is higher than 8, given the diminished quality of the soil moisture data over very cold or arid regions (O and Orth 2021). We only consider the most extreme drought events, as we assume this is associated with the most informative drought–heat signals. We repeat the main analysis using nth extreme droughts and the results remain similar.

c. Bioclimatic regime definition

We classify the climate-vegetation regime of each grid pixel based on its aridity index and tree cover dominance. Using ERA5 data, the aridity index is computed as a ratio of averaged net radiation (expressed in mm) to precipitation over the 15 years. Tree cover dominance is defined as a ratio of tree cover fraction to the total vegetation cover (tree and short vegetation) using the data from the AVHRR vegetation continuous fields products from 2007 to 2016 (Song et al. 2018).

d. Sensitivity and correlation

To examine the relationship between considered variables and temperature increases during drought, we examine the slope of the multiple linear regressions, which can be defined as the sensitivity of temperature to net radiation, or latent heat: temperature = $\alpha \times$ net radiation + $\beta \times$ latent heat + intercept, where α and β are sensitivities of net radiation and latent heat, respectively. We also examine the correlations between the variables, such as the partial correlation coefficient (Pearson's correlation coefficient) of temperature and net radiation while controlling for the effect of latent heat, and vice versa. Both sensitivity and correlation are computed at each grid pixel using the values over the drought period of 51 days (i.e., −50 to 0 days).

3. Elevated temperatures during droughts

We select the most extreme drought event per grid pixel based on the lowest soil moisture value (0–50 cm) and analyze daily maximum temperature anomalies on the day of the drought peak; anomalies are normalized by the standard deviation across temperatures from the same calendar day over all years. As shown in Fig. 1a, most grid pixels show positive temperature anomalies, indicating drought peaks accompanied by elevated temperatures. Nonetheless, we also observe a few negative temperature anomalies, particularly in some arid regions. This could suggest different drought–temperature processes over the regions (e.g., higher albedo during drought results in lower net radiation and therefore decreased temperature).

We further examine the composite temporal variation of the normalized anomalies of soil moisture, temperature, net radiation, and latent heat during the 50-day period before and on the day of the drought peak. Results are shown as median values across grid pixels in humid and arid regions in Figs. 1b and 1c, respectively. Dry anomalies of soil moisture continuously intensify during the drought, as well as warm temperature anomalies, showing a similar temporal pattern of drought–heat development in both regions. Humid regions
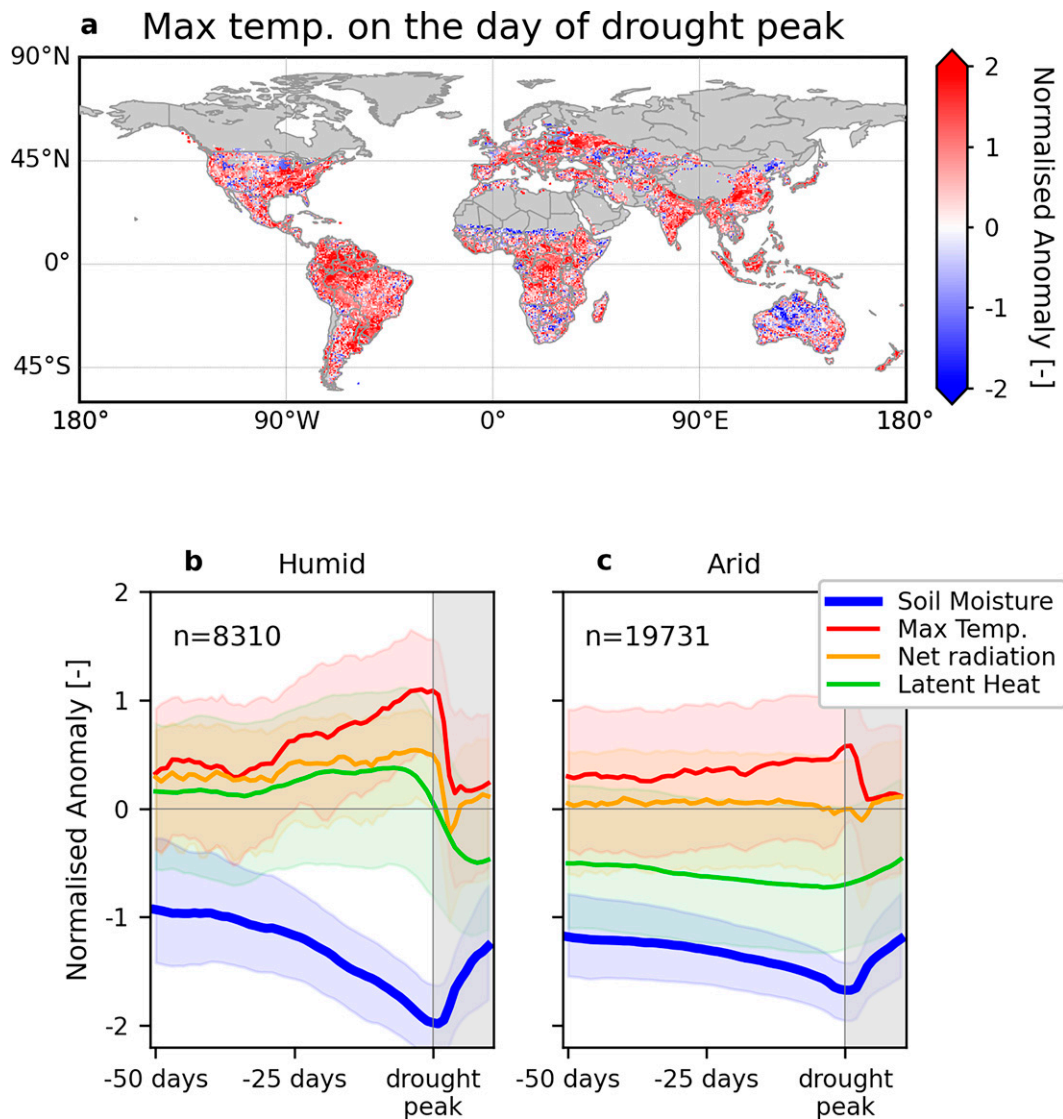
FIG. 1. Widespread elevated temperatures during droughts. (a) Maximum temperature on the day of soil moisture minimum. Temporal evolution of soil moisture, temperature, net radiation, and latent heat during droughts in (b) humid and (c) arid regions. All variables are expressed as normalized anomalies. The aridity index, the ratio of long-term-average net radiation to precipitation, is used to separate humid (≤1) and arid regions (>1). Lines show median values and shading denotes the interquartile range across grid-cell values. A period of 50 days before and including the day of drought peak [unshaded period in (b) and (c)] is considered for further analysis.

dry down faster, and eventually the dry anomaly at the drought peak is stronger than in arid regions. Similarly, the warm temperature anomaly around the drought peak is stronger in humid regions. After the drought peak, the temperature returns to normal within a few days, while soil moisture exhibits a much slower recovery rate owing to its memory effect (Orth and Seneviratne 2012; McColl et al. 2017).

On the other hand, the temporal evolution of net radiation and latent heat anomalies shows remarkably different patterns between the regions (Figs. 1b and 1c), indicating different physical processes involved in drought–heat evolution. In humid regions, net radiation anomalies increase slowly

but continuously until the peak of drought. By contrast, in arid regions, there is almost no net radiation anomaly during the drought period. Latent heat also shows a contrasting temporal variation between the regions, with positive and negative anomalies dominating in humid and arid regions, respectively. In humid and therefore energy-limited regions, vegetation can benefit from increased radiation and hence more available energy during the early stage of drought (Orth and Destouni 2018). However, as the drought peak approaches, latent heat decreases significantly (around 5–7 days before the peak), probably due to reduced vegetation activity resulting from depleted plant-available water. Nonetheless,

positive latent heat values can still be observed over many grid pixels. The relationship between latent heat and temperature anomalies is discussed further in the following section. The situation is different for arid regions. There is generally less water in the soils, such that the latent heat anomaly in those regions is already negative in the early stage of the drought and remains so over the whole drought period.

4. Climatic and vegetation controls of drought-related heat

Radiation partitioning or evaporative cooling can directly affect local temperature changes during drought through the energy and water balances between land and atmosphere. To determine the relative roles of climate and vegetation in such land–atmosphere interactions, we further analyze temperature, net radiation, and latent heat anomalies on the day of the local drought peaks across bioclimatic regimes. These regimes are characterized for each grid pixel using aridity index (the ratio between long-term-average net radiation and precipitation) and tree-cover dominance (the ratio of tree cover to the total tree and short vegetation cover). The global distribution of the regimes can be found from Fig. S1 in the online supplemental material. While short vegetation such as grasses and croplands can occur across regions of diverse aridity levels, trees are prevalent in humid and semiarid regions. For each bioclimatic regime, the median values across grid pixels belonging to the respective regime are reported (Fig. 2). Temperature increases in all regimes, with the strongest warming in subhumid regions (aridity index 0.5–1.0). In general, tree-dominated regions tend to show slightly higher temperature increases. Conversely, arid and grass-dominated regions exhibit relatively small temperature increases.

Some pixels exhibit negative temperature anomalies during peak drought (Fig. 1), which is in contrast to the typical soil moisture–temperature feedback during droughts (Miralles et al. 2019). We find that those negative anomalies are mainly observed in the very arid regions (Fig. S2). This could be due to negative net radiation induced by, for example, higher albedo or increased longwave radiation, but it may also be artifacts due to the use of observation-based datasets, which has relatively large uncertainty in those areas, or the lack of strong drought events during the short study period. At any rate, given the limited impacts of these pixels on the large-scale patterns (Fig. 2a), we retain them in our analysis.

Drought-related net radiation and latent heat anomalies show similar patterns with gradients along aridity and tree dominance (Figs. 2b and 2c, respectively). Net radiation increases (positive anomaly) in most regions, except in the most arid regions with few trees. This net radiation surplus is intuitive; droughts are associated with clear-sky conditions that favor more incoming solar radiation, and hence higher net radiation. The positive net radiation anomalies in general decrease toward arid and grass-dominated regions, which is largely consistent with the spatial pattern of anomalies of incoming shortwave radiation (Fig. S3). Given that the incoming shortwave radiation anomaly is positive globally, negative net radiation anomaly in very arid regions is likely
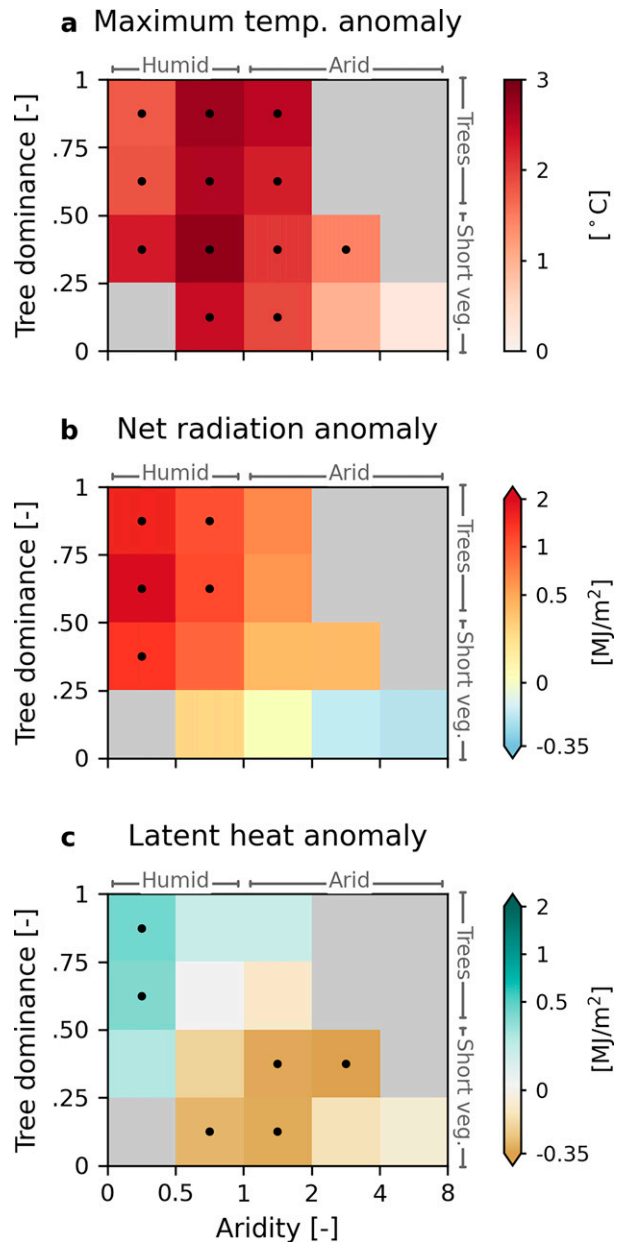

FIG. 2. Anomalies of (a) maximum temperature, (b) net radiation, and (c) latent heat on the day of drought peak across climate–vegetation regimes. Each box shows the median of values across grid pixels within the same regime, defined by long-term aridity and tree-cover dominance. Regime boxes with less than 100 grid pixels are discarded and shown in gray. Black dots within the boxes denote that more than 75% of grid pixels in the regime have the same sign.

attributable to increased outgoing radiation. This is related to drought-associated albedo increases, for example, over water-stressed short vegetation or dry bare soil (Lobell and Asner 2002; Tollerud et al. 2020), which are both more widespread in arid regions. Surface temperature changes may also play a role in modulating outgoing radiation, but

this is not explicitly analyzed in our study mainly due to the lack of suitable observation-based datasets.

The relations between vegetation and temperature during drought can be inferred from the latent heat anomalies in Fig. 2c. In very humid regions, latent heat increases under dry conditions, as seen in Fig. 1b; an excess of net radiation during a drought may promote vegetation activity in such energy-limited conditions (Nicolai-Shaw et al. 2017; Orth and Destouni 2018). Moreover, trees are able to exploit soil water from deep soil layers, maintaining high evaporative cooling (Ellison et al. 2017). Latent heat over subhumid, tree-dominated regions also increases slightly; however, it is not significant given that more than 25% of grid pixels in the regime show (weak) opposite latent heat flux anomalies. In such transitional regions with seasonally dry periods, trees tend to conserve water by reducing the opening of their stomata so as to maintain leaf water potential (Teuling et al. 2010; Vicente-Serrano et al. 2013). By contrast, less tree-dominated regions in all aridity ranges, except <0.5, are associated with reduced latent heat, as short vegetation with shallow roots does not have access to deep soil water and tends not to have water conservation mechanisms (Teuling et al. 2010) and therefore dies as near-surface soils dry below critical levels. The reduced latent heat resulting from dry soils covered with drought-damaged vegetation is consistent with the smaller increase in net radiation (i.e., increased albedo) observed for these regions. No significant change in latent heat is observed in very arid regions (aridity > 4), probably due to a lack of soil moisture in sustaining significant vegetation cover. Our results show the necessity of considering both meteorological and land surface effects (e.g., radiation and vegetation) in order to adequately explain the magnitude of elevated local temperature during droughts, especially in humid forests and semiarid grasslands.

We note that by construction our analysis pools together grid cells that probably experienced droughts of different magnitudes during the study period. To understand the role of drought magnitude for our results, we repeat the analysis by selecting the third and fifth strongest soil moisture droughts at each grid cell. Droughts are considered independent events if the soil moisture minima are at least 180 days apart from each other. We find similar results, although the anomalies of variables become weaker (Fig. S4). Additionally, we repeat our analysis over two subregions, tropical versus temperate climate regions (Fig. S5), and we find that overall spatial patterns of the anomalies remain similar. This implies that the spatial variation of temperature found in this study can be explained by the role of local climate and vegetation, rather than by the large-scale climate or circulation.

5. Contrasting drought–heat pathways between bioclimatic regimes

Next, we examine the interacting mechanisms of net radiation and latent heat related to elevated temperatures during droughts. For this purpose, we compute the temperature sensitivity to net radiation and latent heat, each expressed by the respective slope obtained from a multivariate linear regression using the values over the 50-day period prior to and including the day of drought peak. In addition, to further determine the extent to which the temperature rise is related to each variable, we examine the partial correlation coefficients between net radiation, or latent heat, and temperature. Partial correlation is considered to account for the confounding effect between net radiation and latent heat.

We find a positive relationship between temperature and net radiation (Fig. 3a) with a higher sensitivity in humid regions ranging between $0.41°$ and $0.76°C$ MJ^{-1}, while it decreases toward arid regions ($0.19°$–$0.61°C$ MJ^{-1}). This pattern is supported by the partial correlation results in Fig. 3c. The sensitivity pattern across the bioclimatic regimes is reversed in the case of latent heat (Fig. 3b); the highest absolute sensitivity is observed in arid regions. This can explain why arid regions (aridity ≥ 2) show positive temperature anomalies despite the (weak) cooling effects of negative net radiation (Fig. 2). In humid regions, the sign of the sensitivity and correlation between temperature and latent heat is positive (Figs. 3b and 3d, respectively), indicating that higher latent heat corresponds to higher temperatures. This is not a causal relationship, but an artifact of the increased net radiation. Positive net radiation does not only lead to increased sensible heat flux and consequently temperature, but also to elevated latent heat. In humid regions, there can be soil moisture available for evapotranspiration even during drought events (Fig. S6). As a result, the evaporative cooling decelerates the rate of temperature increase while the temperature anomaly remains positive. We warn that high correlation does not imply causation. Additionally, we find significant ($p < 0.1$) evidence of Granger causality (Granger 1969) between net radiation/latent heat and temperature anomalies from most grid pixels (Fig. S7). Nonetheless, the Granger causality test does not rule out the possibility of a confounding variable and only provides information about forecasting ability. Therefore, in future research, it would be interesting to test detailed cause-and-effect hypotheses including more explanatory variables or using more alternative techniques.

Sensitivities of temperature to net radiation are generally lower than in the case of latent heat. This can be explained as the radiative energy is not exclusively translated into sensible heat flux and consequently temperature increase, but it is also partitioned into latent and ground storage energy fluxes. When it comes to the sensitivity of temperature to latent heat, the very high absolute sensitivity over very arid regions (aridity ≥ 2) is observed; it takes less energy to heat dry air than wet air and absolute humidity during droughts is much lower in arid regions (Fig. S8). We note, however, that our analysis does not include the effect of advected warm or cold air masses, such as due to drought-characteristic atmospheric circulation anomaly patterns (Schumacher et al. 2019). While the sensitivity and partial correlation results generally agree, we find an overall weaker partial correlation between temperature and latent heat than between temperature and net radiation (0.02–0.42 and 0.06–0.67 in absolute terms, respectively), opposite to the sensitivity magnitudes. This could be related to higher uncertainties and consequently more noise in the large-scale latent heat estimates compared with the possibly better constrained net radiation estimates. We additionally calculate sensitivity
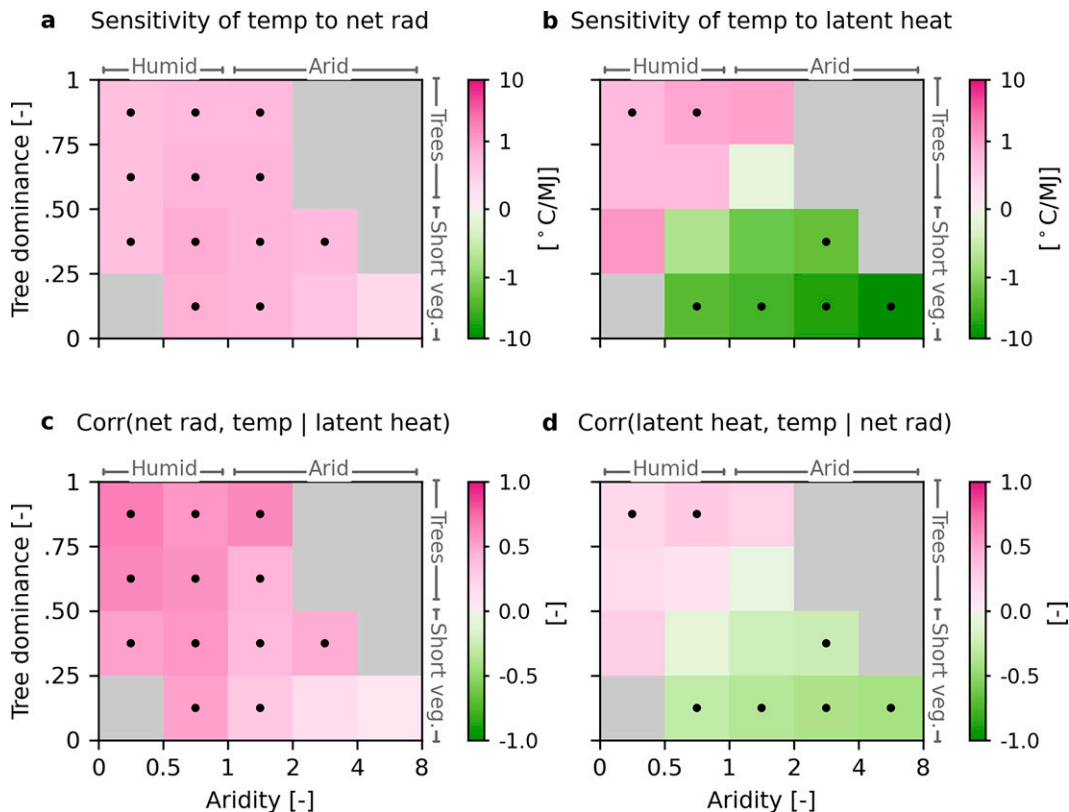
FIG. 3. Contrasting effects of net radiation and latent heat flux on drought temperatures. Sensitivity of temperature anomalies to (a) net radiation anomalies and (b) latent heat anomalies. (c) Partial correlation coefficient between temperature and net radiation while controlling for latent heat. (d) Partial correlation coefficient between temperature and latent heat while controlling for net radiation. Values are first computed at each grid pixel over the 51-day window prior to, and including, drought peak; then the median is calculated across grid pixels within the same climate–vegetation regime. Black dots within the boxes denote that more than 75% of grid pixels in the regime have the same sign.

and correlation using the drought period of −25 to 0 days and find that the results remain the same (Fig. S9).

Our results show that temperature anomalies during drought should be understood from a comprehensive assessment of the interplay between meteorological and land processes including vegetation effects, which vary across bioclimatic regimes in magnitude, sign, and relative importance. For instance, while during drought net radiation increases most strongly in very humid regions, it is buffered by coinciding latent heat increases. In contrast, in subhumid regions, net radiation increases less, but combined with the decrease in latent heat, results in the largest increases in temperature over short vegetation regions. This is the case also for tree-dominated regions; forests' evaporative cooling is buffering net radiation increases less in subhumid than in very humid regions. Consequently, we observe the strongest temperature anomalies over subhumid climates.

6. Conclusions and discussion

In summary, our findings indicate contrasting drought–heat pathways between climate–vegetation regimes (Fig. 4). In humid and subhumid regions, warming during droughts is largely

driven by a drought-related net radiation surplus. In contrast, a less significant change in temperature is found in arid regions as there is even a small net radiation deficit during droughts, caused by a smaller surplus in incoming shortwave radiation, which is (over)compensated by higher albedo over a dried-out, brighter surface. Meanwhile, the role of vegetation and evaporative cooling in complementing those mechanisms is of importance in transitional climate regimes (subhumid and semiarid regions), leading to significant drought-related warming in these regions. Thereby, short vegetation amplifies the drought-related warming predominantly in transitional regions, but less so in arid regions, where it generally cannot control evaporative fraction due to a lack of absolute soil water. On the other hand, forests with deeper rooting systems become water-stressed less frequently in transitional regimes, where they consequently cause the strongest drought warming amplification. As a result, our findings show that background climate and vegetation conditions determine the magnitude of contributions from these mechanisms, highlighting the importance of considering all interacting factors in understanding concurrent drought–heat extremes.
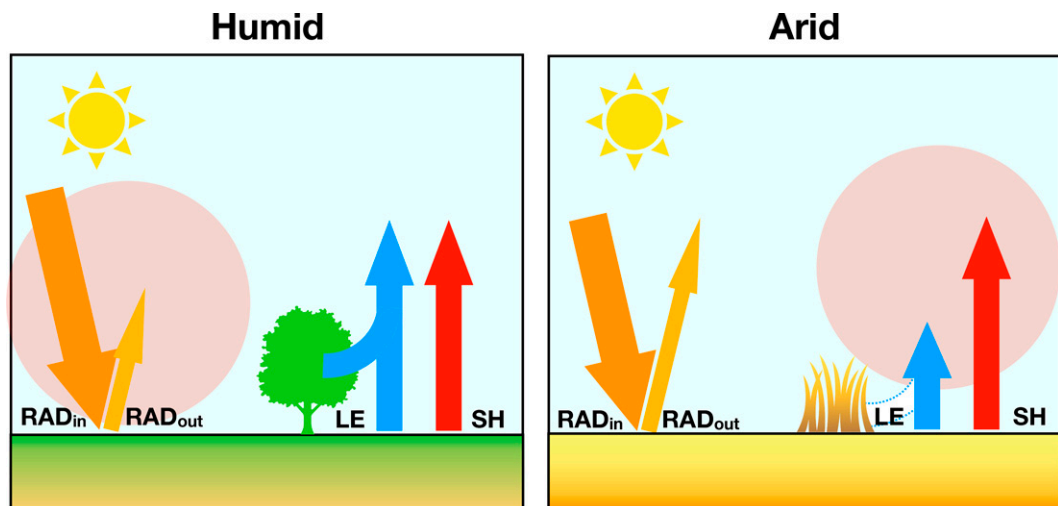
FIG. 4. Schematic summary of dominant drought–heat pathways in different climate regions. (left) During drought, increased incoming radiation ($RAD_{in} > RAD_{out}$), and consequently increased net radiation, leads to warm temperature anomalies in humid regions, despite the buffering effect of concurrently increased surface latent heat fluxes (LE). (right) On the other hand, net radiation increases are smaller in arid regions, for instance, due to enhanced outgoing shortwave radiation by increased albedo related to reduced soil moisture and dry vegetation. However, the water-limited conditions limit LE, leading to larger sensible heat fluxes (SH) and therefore elevated temperature.

The main datasets employed in this study are produced using machine learning trained with in situ measurement. This enables us to investigate the temporal and spatial variations of land surface variables largely based on observations, as the ML-driven data are independent of model assumptions (e.g., on the parameterization of plant water stress and soil properties), which might be imperfect due to our limited knowledge about the complex relationships between soil moisture, vegetation, and energy fluxes (Verhoef and Egea 2014; Teodosio et al. 2017). However, at the same time, machine learning cannot benefit from physics knowledge and therefore, the performance of such machine learning-based data is significantly affected by the quality and diversity of training data. Our previous study shows the reliability of machine learning highly depends on the diversity of training data (O et al. 2020a). In this sense, the performance of SoMo.ml, which is derived from machine learning trained with in situ data, is relatively poor over high northern latitudes and desert areas due to insufficient training data. This possibly leads to artifact signals in this study. However, this is not expected to affect our conclusions as we focus on the spatially averaged patterns using large numbers of grid pixels from similar bioclimatic regimes around the globe so that errors are in principle canceled out. Consequently, our results offer observational evidence for the spatial patterns of drought–heat relevant variables that can reveal opportunities to improve modeling and input data quality. Future work should test the consistency of our key findings among different observational datasets or physically based model outputs.

As a compound event, drought and heat can jointly lead to severe, multifaceted consequences across socioeconomic sectors (Brown 2016; Di Napoli et al. 2018; Orth and Destouni 2018; Orth et al. 2022). While our study provides valuable inputs to better understand the drought–heat pathways and their spatial variations, the evolution of these pathways in a changing future climate remains elusive. For instance, changes in cloud cover might affect drought-related vegetation anomalies, while continued vegetation greening or CO_2 fertilization could alter the evaporative cooling signals (Peters et al. 2018; Schneider et al. 2019). Thus, while our results provide a broader perspective of drought–heat extremes, they also call for further investigation of drought-related warming processes in both historical climate model simulations as well as projections, as this is crucial to predict the drought–heat pathways in a warmer world.

Data availability statement. All datasets used in this study are publicly available from the references indicated. All data generated and/or analyzed during this study are available from the corresponding author on reasonable request.

REFERENCES

Alizadeh, M. R., and Coauthors, 2020: A century of observations reveals increasing likelihood of continental-scale compound dry-hot extremes. *Sci. Adv.*, **6**, eaaz4571, https://doi.org/10.1126/sciadv.aaz4571.

Anderegg, W. R. L., A. T. Trugman, D. R. Bowling, G. Salvucci, and S. E. Tuttle, 2019: Plant functional traits and climate influence drought intensification and land–atmosphere feedbacks. *Proc. Natl. Acad. Sci. USA*, **116**, 14071–14076, https://doi.org/10.1073/pnas.1904747116.

Bastos, A., and Coauthors, 2020: Direct and seasonal legacy effects of the 2018 heat wave and drought on European ecosystem productivity. *Sci. Adv.*, **6**, eaba2724, https://doi.org/10.1126/sciadv.aba2724.

Below, R., E. Grover-Kopec, and M. Dilley, 2007: Documenting drought-related disasters: A global reassessment. *J. Environ. Dev.*, **16**, 328–344, https://doi.org/10.1177/1070496507306222.

Brown, A., 2016: Heatwave mortality. *Nat. Climate Change*, **6**, 821., https://doi.org/10.1038/nclimate3117.

Cheng, L., M. Hoerling, Z. Liu, and J. Eischeid, 2019: Physical understanding of human-induced changes in U.S. hot droughts using equilibrium climate simulations. *J. Climate*, **32**, 4431–4443, https://doi.org/10.1175/JCLI-D-18-0611.1.

Chiang, F., O. Mazdiyasni, and A. AghaKouchak, 2018: Amplified warming of droughts in southern United States in observations and model simulations. *Sci. Adv.*, **4**, eaat2380, https://doi.org/10.1126/sciadv.aat2380.

Ciais, Ph., and Coauthors, 2005: Europe-wide reduction in primary productivity caused by the heat and drought in 2003. *Nature*, **437**, 529–533, https://doi.org/10.1038/nature03972.

Di Napoli, C., F. Pappenberger, and H. L. Cloke, 2018: Assessing heat-related health risk in Europe via the Universal Thermal Climate Index (UTCI). *Int. J. Biometeor.*, **62**, 1155–1165, https://doi.org/10.1007/s00484-018-1518-2.

Ellison, D., and Coauthors, 2017: Trees, forests and water: Cool insights for a hot world. *Global Environ. Change*, **43**, 51–61, https://doi.org/10.1016/j.gloenvcha.2017.01.002.

Fink, A. H., T. Brücher, A. Krüger, G. C. Leckebusch, J. G. Pinto, and U. Ulbrich, 2004: The 2003 European summer heatwaves and drought—Synoptic diagnosis and impacts. *Weather*, **59**, 209–216, https://doi.org/10.1256/wea.73.04.

Flach, M., and Coauthors, 2018: Contrasting biosphere responses to hydrometeorological extremes: Revisiting the 2010 western Russian heatwave. *Biogeosciences*, **15**, 6067–6085, https://doi.org/10.5194/bg-15-6067-2018.

Granger, C. W. J., 1969: Investigating causal relations by econometric models and cross-spectral methods. *Econometrica*, **37**, 424–438, https://doi.org/10.2307/1912791.

Grossiord, C., T. N. Buckley, L. A. Cernusak, K. A. Novick, B. Poulter, R. T. W. Siegwolf, J. S. Sperry, and N. G. McDowell, 2020: Plant responses to rising vapor pressure deficit. *New Phytol.*, **226**, 1550–1566, https://doi.org/10.1111/nph.16485.

Hauser, M., R. Orth, and S. I. Seneviratne, 2016: Role of soil moisture versus recent climate change for the 2010 heat wave in western Russia. *Geophys. Res. Lett.*, **43**, 2819–2826, https://doi.org/10.1002/2016GL068036.

Hersbach, H., and Coauthors, 2020: The ERA5 global reanalysis. *Quart. J. Roy. Meteor. Soc.*, **146**, 1999–2049, https://doi.org/10.1002/qj.3803.

Hirschi, M., and Coauthors, 2011: Observational evidence for soil-moisture impact on hot extremes in southeastern Europe. *Nat. Geosci.*, **4**, 17–21, https://doi.org/10.1038/ngeo1032.

Jung, M., and Coauthors, 2019: The FLUXCOM ensemble of global land–atmosphere energy fluxes. *Sci. Data*, **6**, 74, https://doi.org/10.1038/s41597-019-0076-8.

Lobell, D. B., and G. P. Asner, 2002: Moisture effects on soil reflectance. *Soil. Sci. Soc. Amer. J.*, **66**, 722–727, https://doi.org/10.2136/sssaj2002.7220.

Matheny, A. M., and Coauthors, 2015: Observations of stem water storage in trees of opposing hydraulic strategies. *Ecosphere*, **6**, art165, https://doi.org/10.1890/ES15-00170.1.

Mazdiyasni, O., and A. AghaKouchak, 2015: Substantial increase in concurrent droughts and heatwaves in the United States. *Proc. Natl. Acad. Sci. USA*, **112**, 11484–11489, https://doi.org/10.1073/pnas.1422945112.

McColl, K. A., and Coauthors, 2017: The global distribution and dynamics of surface soil moisture. *Nat. Geosci.*, **10**, 100–104, https://doi.org/10.1038/ngeo2868.

Miralles, D. G., P. Gentine, S. I. Seneviratne, and A. J. Teuling, 2019: Land–atmospheric feedbacks during droughts and heatwaves: State of the science and current challenges. *Ann. N. Y. Acad. Sci.*, **1436**, 19–35, https://doi.org/10.1111/nyas.13912.

Mueller, B., and S. I. Seneviratne, 2012: Hot days induced by precipitation deficits at the global scale. *Proc. Natl. Acad. Sci. USA*, **109**, 12398–12403, https://doi.org/10.1073/pnas.1204330109.

Nicolai-Shaw, N., J. Zscheischler, M. Hirschi, L. Gudmundsson, and S. I. Seneviratne, 2017: A drought event composite analysis using satellite remote-sensing based soil moisture. *Remote Sens. Environ.*, **203**, 216–225, https://doi.org/10.1016/j.rse.2017.06.014.

O, S., and R. Orth, 2021: Global soil moisture data derived through machine learning trained with in-situ measurements. *Sci. Data*, **8**, 170, https://doi.org/10.1038/s41597-021-00964-1.

——, E. Dutra, and R. Orth, 2020a: Robustness of process-based versus data-driven modeling in changing climatic conditions. *J. Hydrometeor.*, **21**, 1929–1944, https://doi.org/10.1175/JHM-D-20-0072.1.

——, Hou, X., and R. Orth, 2020b: Observational evidence of wildfire-promoting soil moisture anomalies. *Sci. Rep.*, **10**, 11008, https://doi.org/10.1038/s41598-020-67530-4.

Orth, R., and S. I. Seneviratne, 2012: Analysis of soil moisture memory from observations in Europe. *J. Geophys. Res.*, **117**, https://doi.org/10.1029/2011JD017366.

——, and G. Destouni, 2018: Drought reduces blue-water fluxes more strongly than green-water fluxes in Europe. *Nat. Commun.*, **9**, 3602, https://doi.org/10.1038/s41467-018-06013-7.

——, and Coauthors, 2022: Contrasting biophysical and societal impacts of hydro-meteorological extremes. *Environ. Res. Lett.*, **17**, 014044, https://doi.org/10.1088/1748-9326/ac4139.

Peters, W., and Coauthors, 2018: Increased water-use efficiency and reduced CO_2 uptake by plants during droughts at a continental scale. *Nat. Geosci.*, **11**, 744–748, https://doi.org/10.1038/s41561-018-0212-7.

Santanello, J. A., and Coauthors, 2018: Land–atmosphere interactions: The LoCo perspective. *Bull. Amer. Meteor. Soc.*, **99**, 1253–1272, https://doi.org/10.1175/BAMS-D-17-0001.1.

Schneider, T., C. M. Kaul, and K. G. Pressel, 2019: Possible climate transitions from breakup of stratocumulus decks under

greenhouse warming. *Nat. Geosci.*, **12**, 163–167, https://doi.org/10.1038/s41561-019-0310-1.

Schumacher, D. L., and Coauthors, 2019: Amplification of mega-heatwaves through heat torrents fuelled by upwind drought. *Nat. Geosci.*, **12**, 712–717, https://doi.org/10.1038/s41561-019-0431-6.

Shadman, F., S. Sadeghipour, M. Moghavvemi, and R. Saidur, 2016: Drought and energy security in key ASEAN countries. *Renew. Sustain. Energy Rev.*, **53**, 50–58, https://doi.org/10.1016/j.rser.2015.08.016.

Sharma, S., and P. Mujumdar, 2017: Increasing frequency and spatial extent of concurrent meteorological droughts and heatwaves in India. *Sci. Rep.*, **7**, 15 582, https://doi.org/10.1038/s41598-017-15896-3.

Song, X. P., and Coauthors, 2018: Global land change from 1982 to 2016. *Nature*, **560**, 639–643, https://doi.org/10.1038/s41586-018-0411-9.

Teodosio, B., V. R. N. Pauwels, S. P. Loheide, and E. Daly, 2017: Relationship between root water uptake and soil respiration: A modeling perspective. *J. Geophys. Res. Biogeosci.*, **122**, 1954–1968, https://doi.org/10.1002/2017JG003831.

Teuling, A. J., 2018: A hot future for European droughts. *Nat. Climate Change*, **8**, 364–365, https://doi.org/10.1038/s41558-018-0154-5.

——, and S. I. Seneviratne, 2008: Contrasting spectral changes limit albedo impact on land–atmosphere coupling during the 2003 European heat wave. *Geophys. Res. Lett.*, **35**, L03401, https://doi.org/10.1029/2007GL032778.

——, and Coauthors, 2010: Contrasting response of European forest and grassland energy exchange to heatwaves. *Nat. Geosci.*, **3**, 722–727, https://doi.org/10.1038/ngeo950.

Tollerud, H. J., J. F. Brown, and T. R. Loveland, 2020: Investigating the effects of land use and land cover on the relationship between moisture and reflectance using Landsat time series. *Remote Sens.*, **12**, 1919, https://doi.org/10.3390/rs12121919.

Verhoef, A., and G. Egea, 2014: Modeling plant transpiration under limited soil water: Comparison of different plant and soil hydraulic parameterizations and preliminary implications for their use in land surface models. *Agric. For. Meteor.*, **191**, 22–32, https://doi.org/10.1016/j.agrformet.2014.02.009.

Vicente-Serrano, S. M., and Coauthors, 2013: Response of vegetation to drought time-scales across global land biomes. *Proc. Natl. Acad. Sci. USA*, **110**, 52–57, https://doi.org/10.1073/pnas.1207068110.

Wilhite, D. A., 2000: Drought as a natural hazard: Concepts and definitions. *Drought: A Global Assessment*, Vol. 1, Routledge, 1–18.

Yu, R., and P. Zhai, 2020: More frequent and widespread persistent compound drought and heat event observed in China. *Sci. Rep.*, **10**, 14576, https://doi.org/10.1038/s41598-020-71312-3.